Taylor & Francis
Taylor & Francis Group

Phase Transitions
A Multinational Journal

ISSN: 0141-1594 (Print) 1029-0338 (Online) Journal homepage: http://www.tandfonline.com/loi/gpht20

Anisotropy of acoustic and thermal expansion properties of $TlInSe_2$ crystals

I. Martynyuk-Lototska, O. Mys, A. Say, I. Trach, D. Adamenko, O. O. Gomonnai, I. Roman & R. Vlokh

To cite this article: I. Martynyuk-Lototska, O. Mys, A. Say, I. Trach, D. Adamenko, O. O. Gomonnai, I. Roman & R. Vlokh (2019) Anisotropy of acoustic and thermal expansion properties of $TlInSe_2$ crystals, Phase Transitions, 92:1, 23-35, DOI: 10.1080/01411594.2018.1545227

To link to this article: https://doi.org/10.1080/01411594.2018.1545227

Published online: 19 Nov 2018.

PHASE TRANSITIONS
2019, VOL. 92, NO. 1, 23–35
https://doi.org/10.1080/01411594.2018.1545227

Taylor & Francis
Taylor & Francis Group

Anisotropy of acoustic and thermal expansion properties of $TlInSe_2$ crystals

I. Martynyuk-Lototska[a], O. Mys[a], A. Say[a], I. Trach[b], D. Adamenko[a], O. O. Gomonnai[a,c], I. Roman[d] and R. Vlokh[a]

[a]Vlokh Institute of Physical Optics, Lviv, Ukraine; [b]Hetman Petro Sahaidachnyi National Army Academy, Lviv, Ukraine; [c]Department of Physics, Uzhhorod National University, Uzhhorod, Ukraine; [d]Institute of Electron Physics of National Academy of Sciences of Ukraine, Uzhhorod, Ukraine

ABSTRACT

Based on experimental studies of acoustic wave velocities in $TlInSe_2$ crystals, all components of their elastic stiffness and compliance tensors are determined. $TlInSe_2$ has three acoustic axes parallel to the principal crystallographic directions. The lowest velocities of acoustic eigenwaves are used to estimate the acousto-optic figure of merit. We analyse deviations from purely longitudinal and transverse polarization states, as well as the obliquity of acoustic energy flow. Temperature dependences of strains along the three principal crystallographic directions and of acoustic wave velocities v_{11}, v_{22} and v_{33} are measured. Anomalous behaviour of these parameters occur at $T_1C_{11} = C_{33}245$ K and $T_2C_{12} = C_{13}145$ K. It is shown that the symmetry of $TlInSe_2$ becomes lower than tetragonal below the temperature point T_1.

ARTICLE HISTORY
Received 16 July 2018
Accepted 29 October 2018

KEYWORDS
Ferroics; thermal expansion; acoustic wave velocity; elastic properties; anisotropy; $TlInSe_2$ crystals

1. Introduction

$TlInSe_2$ crystals belong to the group of ternary thallium halcogenides with a general formula $TlMX_2$ (M = Ga, In; X = Se, S, Te). They are characterized by layered or chain-like low-dimensional structures [1]. For instance, monoclinic $TlGaS_2$, $TlInS_2$ and $TlGaSe_2$ have a layered structure [2–4], while tetragonal $TlGaTe_2$, $TlInTe_2$ and $TlInSe_2$ compounds crystallize in a chain structure [5]. Both types of crystals belong to the same group of $A^{III}B^{III}C_2^{IV}$ semiconductors. Most of the layered crystals of this family are proper ferroelectrics, with an incommensurate (IC) phase between the para and ordered phase. These crystals undergo phase transitions (PTs) with symmetry change 2/m ↔ IC ↔ 2 (see, e.g. the review [1]). However, the PTs are not fully understood. For example, it has been found that the layered $TlInS_2$ crystals show metastable polytype structures and, as a result of polytypism, anomalies of their physical parameters appear at further temperatures. These anomalies correspond to various polytypes that are characterized by multiplication of the c lattice parameter with $c = 2c^*$, $4c^*$, $8c^*$ and $16c^*$, where $c^* = 15.18$ Å [6–10].

PTs are even more complex for chain-type tetragonal crystals. Using the studies of the heat capacity, the lattice parameters and the intensities of X-ray Bragg reflections, a second-order PT at 98.5 K has been detected in $TlGaTe_2$ crystals [11] but not in other compounds in this group. Here the modulated IC structure has been assumed to exist at the temperatures above 98.5 K (110–290 K). A number of temperature intervals with temperature independent lattice parameter a exist between 110 and 290 K. This behaviour has been explained as a so-called 'devil's staircase' [11]. $TlGaTe_2$ has been studied down to temperatures of 5 K, with no additional PTs observed.

CONTACT R. Vlokh vlokh@ifo.lviv.ua

The existence of a non-ferroelectric PT at 98.5 K in $TlGaTe_2$ has been confirmed by some other studies (see, e.g. [12,13]). As a result, several questions arise: (i) what is the nature of the phase below 98.5 K? (ii) Is the phase above 98.5 K incommensurate or do different phases coexist in the temperature region 98.5–290 K? (iii) What is the temperature of a para-to-IC PT, in case that the IC phase really exists?

PTs in $TlInSe_2$ are even less clear. The authors of the study [14] have not found an anomaly in the heat capacity in the region 170–215 K, although anomalies of the dielectric permittivity and the conductivity have reported at 210, 200 and 196.8 K [15]. Other PTs in $TlInSe_2$ at 135 and 185 K were reported by Ref. [16] from the temperature dependence of the lattice parameter *a*. Alekperov et al. [17] reported anomalies at 135 and 185 K in the temperature dependence of the photoconductivity, the lattice parameter *a*, and the heat capacity of $TlInSe_2$. They have suggested that the interval in between these points corresponds to the IC phase. The anomaly of the heat capacity at 185 K is more pronounced than the small diffused maximum observed at 135 K [17]. This does not agree with the fact that, usually, the para-to-IC PT and the IC-to-ordered PTs are of the second and first orders, respectively.

Although the X-ray studies of $TlInSe_2$ have been carried out in several contributions, so-called satellite reflections corresponding to the superstructure have not been found ([18]), neither have they been found in [19]. However, Hosokawa et al. [19] have proposed an unusual concept of the IC phase. They suppose that the positions of Tl atoms fluctuate significantly with respect to the $InSe_4$-chain framework in the IC phase existing above 135 K, although in the commensurate phase below 135 K, these atoms are located with corresponding distances well defined (about 0.34 nm). This reflects a fact that the phase is perfectly ordered. According to [20], Tl atoms produce periodical one-dimensional arrays relative to In and Se_2 layers in the para phase, and the periodicity becomes broken in the IC phase. On the other hand, no PT has been detected at 185 K in the work [19], although the authors of the study [20] believe that $TlInSe_2$ should reveal a structural PT from the high-temperature normal phase into the IC phase at around 410–460 K, which coincides with the region where a giant thermoelectric effect appears [21].

Following from these contradictory data, one can conclude that the information available on the PTs in $TlInSe_2$ is far from complete. The primary goal of our current work is to continue the studies of PTs in the $TlInSe_2$ crystals. We include in our analysis the anisotropy appearing at the PTs, which should be accompanied by symmetry lowering of the properties under study, in particular, thermal expansion and acoustic wave (AW) velocities. Acoustic properties of $TlInSe_2$ are also studied since the crystal seems to be a promising acousto-optic (AO) material. According to [22], the AO figure of merit (AOFM) for $TlInSe_2$ is equal to 156×10^{-15} s^3/kg at the wavelength 1.15 $C_{44} = C_{66} = (C_{11} - C_{12})/2$ in the case of AO interactions with the longitudinal AW v_{22}. As shown in our recent work [23], the AOFM of $TlInS_2$ can reach very high values, $\sim$ $(2200–9000) \times 10^{-15}$ s^3/kg. This coefficient can increase at the interactions with slower quasi-transverse AWs. In order to analyse the anisotropy of AOFM [24–26], we determine complete matrices of elasto-optic and elastic-stiffness coefficients, which determine the AW velocities. Hence, below we also investigate the anisotropy of acoustic properties of the $TlInSe_2$ crystals.

Let us remind in brief the main properties of $TlInSe_2$, which are needed for our analysis. The $TlInSe_2$ crystals belong to the space symmetry group I4/mcm (point group 4/mmm). Their lattice parameters are $a = 8.075$ Å and $c = 6.847$ Å ($Z = 4$) [5]. $TlInSe_2$ exhibits a giant Peltier–Seebeck effect below 410 K, with the Seebeck coefficient being as high as 10^5–10^7 μV/K at room temperature. It is believed to be related to the IC structure of these crystals [20]. The crystal is transparent in the infrared spectral range at the wavelengths longer than ~1μm (the bandgap $E_g = 1.18$ eV at 300 K) [27]. For the best of our knowledge, the data for the low-energy absorption edge is not available in the literature. The temperature dependence of the linear thermal expansion coefficient has earlier been studied [28]. However, the experimental geometry and, in particular, the orientation of the sample with respect to the crystallographic coordinate system was not given [28] so that comparison with our data is difficult. The refractive indices were studied with an ellipsometric technique [29].

Using a standard Sellmeier approximation and the data reported in [29], we have calculated the refractive indices at 1.15 μm: $n_o = 2.99$ and $n_e = 3.26$.

2. Experimental techniques and procedures

To synthesize and grow the ternary compound $TlInSe_2$ using initial substances of high purity. The synthesis was performed using standard melting methods. The $TlInSe_2$ crystals were grown with a Bridgman–Stockbarger technique at the Institute of Electronic Physics of NAS of Ukraine. The initial substances were loaded into quartz ampoules with the inner diameter of 15–20 mm. They were soldered after reaching the vacuum 10^{-4} mm Hg. The melt of the $TlInSe_2$ compound was crystallized along a horizontal direction. The temperatures were 800–840°C in the melting zone and 690–710°C in the annealing zone. The melting temperature of $TlInSe_2$ is 750°C. The vertical temperature gradient in the zone of crystallization was 3–5°C/mm and the velocity at which the ampoule moved from the melting zone to the annealing zone was 0.10–0.25 mm/h. The crystals in Figure 1 were cooled at the rate of 50–60°C/h. The crystal structure was checked by X-ray diffraction. Our data agreed well with the results in [5]. The directions of the crystallographic axes were determined using the same X-ray method.

The relative thermal expansions $\Delta L_i/L_j^0 = (L_i - L_i^0)/L_j^0$ (with L_i^0 and L_j^0 being the initial sizes of a sample respectively along the directions i and j, and L_i the thermally induced size) were measured with a quartz-capacity dilatometer along the crystallographic axes a, b and c. The thermal expansion tensor $\alpha_{ij} = \partial(\Delta L_i/L_j^0)/\partial T$ for the tetragonal $TlInSe_2$ crystals written in the crystallographic coordinate system is as follows:

$$\alpha_{ij} = \begin{vmatrix} \alpha_{aa} & 0 & 0 \\ 0 & \alpha_{bb} & 0 \\ 0 & 0 & \alpha_{cc} \end{vmatrix}, \tag{1}$$

where $\alpha_{bb} = \alpha_{aa}$. The volume thermal expansion coefficient was determined as $\alpha_V = \alpha_{aa} + \alpha_{bb} + \alpha_{cc}$. The dilatometer was built at the Vlokh Institute of Physical Optics (Lviv, Ukraine). The average sensitivity of our dilatometer was about 2 nm in the region 105–300 K under test. The measurements were carried out in the cooling run, with the temperature scan rate 0.02 K/min. The accuracy of temperature measurements was not worse than 0.01 K. The mean-square error for the thermal expansion coefficients did not exceed $\sim 0.7 \times 10^{-5}$ K^{-1}. The samples for the thermal expansion measurements had the same size as those prepared for the AW-velocity measurements (see below).

We prepared three nearly cubic-shaped samples of $TlInSe_2$ for the AW velocity measurements. The faces of these samples were perpendicular respectively to (1) a, b and c axes, (2) b axis, and directions [101] and [10$\bar{1}$], and (3) c axis, and directions [110] and [1$\bar{1}$0]. The average dimensions of our samples were $\sim 5 \times 5 \times 5$ mm^3. The AW velocities were measured with the error < 2% using a pulse echo-overlap method [30]. We excited the AWs by standard $LiNbO_3$ transducers with the resonance frequency $f = 10$MHz, the bandwidth $\Delta f = 0.1$MHz and the acoustic power $P_a = 1 - 2$W. The

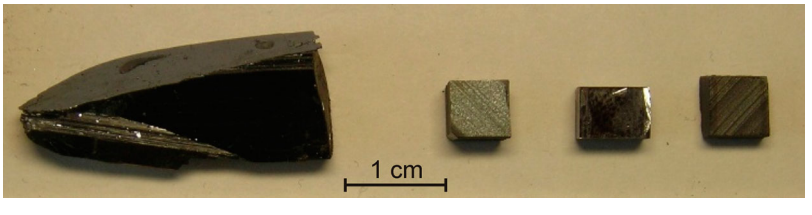

Figure 1. $TlInSe_2$ crystals grown in the present work.

AW velocities were denoted using the indices associated with the crystallographic axes, according to the standard notation $a = 1$, $b = 2$ and $c = 3$.

The elastic-stiffness coefficients were calculated using the AW velocities determined experimentally and the formulae $C_{11} = \rho v_{11}^2$, $C_{33} = \rho v_{33}^2$, $C_{44} = \rho v_{23}^2$, $C_{66} = \rho v_{12}^2$, $C_{12} = 2(\rho v_{66}^2 - C_{66}) - C_{11}$ and $C_{13} = \sqrt{(C_{11} - 2\rho v_{55}^2 + C_{44})(C_{33} - 2\rho v_{55}^2 + C_{44})} - C_{44}$. Here $\rho = 6460\ \mathrm{kg/m^3}$ is the material density determined by us, and v_{ij} the AW velocities (with i and j indicating respectively the propagation and polarization directions of the AW). The elastic compliances were calculated, following from the matrix of elastic-stiffness coefficients and the formulae

$$
\begin{aligned}
&S_{11} = S_{22} = \frac{C_{11}C_{33} - C_{13}^2}{C_{33}C_{11}^2 - 2C_{13}^2C_{11} - C_{12}^2C_{33} + 2C_{13}^2C_{12}}, \qquad S_{33} = \frac{C_{11} + C_{12}}{C_{11}C_{33} - 2C_{13}^2 + C_{12}C_{33}},\\
&S_{12} = \frac{C_{13}^2 - C_{12}C_{33}}{C_{33}C_{11}^2 - 2C_{13}^2C_{11} - C_{12}^2C_{33} + 2C_{13}^2C_{12}}, \quad S_{13} = S_{23} = -\frac{C_{13}}{C_{11}C_{33} - 2C_{13}^2 + C_{12}C_{33}},\\
&S_{55} = S_{44} = 1/C_{44}, \quad S_{66} = 1/C_{66}.
\end{aligned}
\tag{2}
$$

The obliquity angle between the acoustic group-velocity direction and the AW vector was calculated using the relation [31]

$$\Delta_i = \arctan\frac{1}{v(\phi_i)}\frac{\partial v(\phi_i)}{\partial \phi_i}. \tag{3}$$

$v(\phi_i)$ denotes a function of AW velocity that depends upon the angle ϕ_i between the wave vector and the corresponding axis of the crystallographic coordinate system, with the subscript i referring to the axis perpendicular to the geometric plane under consideration.

The angle of deviation of the AW polarization from purely longitudinal types is also a very important characteristic of AO materials. We calculated this angle from the Christoffel equation [32]:

$$\zeta_1 = \frac{1}{2}\arctan\frac{(C_{13} + C_{44})\sin 2\phi_1}{(C_{11} - C_{44})\cos^2\phi_1 + (C_{44} - C_{33})\sin^2\phi_1}, \tag{4}$$

$$\zeta_3 = \frac{1}{2}\arctan\frac{(C_{11} + C_{66})\sin 2\phi_3}{(C_{11} - C_{66})\cos^2\phi_3 + (C_{66} - C_{11})\sin^2\phi_3}. \tag{5}$$

These relations refer respectively to the bc and ab planes. Here ϕ_1 (or ϕ_3) is the angle between the AW vector and the b (or a) axis. The corresponding non-orthogonality of quasi-transverse (QT) waves can be calculated in the same manner, with the only difference that the additive factor of 90° should be added to the r.h.s. of formulae (4) and (5).

For all the data presented in the following figures, the error bars are less or comparable with the diameter of the data points.

3. Results and discussion

3.1. Acoustic and elastic anisotropy

The AW velocities are listed in Table 1. The velocities of quasi-longitudinal (QL) waves are moderate. For QT waves are the velocities of the AWs propagating along the principal crystallographic axes do not exceed 1356 m/s. These velocities predispose high AOFM for $TlInSe_2$, which is proportional to the inverse cube of the AW velocity. Based on the AW velocities determined experimentally, we

Table 1. AW velocities measured for $TlInSe_2$.

ij	11	33	55	66	12	23
v_{ij} (m/s)	2553 ± 25 ($v_{11} = v_{22}$)	3596 ± 30	2838 ± 25	2444 ± 20	1319 ± 12 ($v_{12} = v_{21}$)	1356 ± 15

have calculated a complete matrix of elastic-stiffness coefficients. Table 2 lists also the elastic-compliance coefficients. One can see that the S_{44} and S_{66} coefficients are larger than the other tensor components. This means that the $TlInSe_2$ crystals are very compliant with respect to the shear stresses σ_4, σ_5 and σ_6.

Using the matrix of elastic-stiffness coefficients, we construct the cross sections of the AW velocity surfaces by the principal crystallographic planes. In the *bc* plane, only the velocity of the AW QT_1 does not depend on the propagation direction (see Figure 2(a)). As seen from Figure 2(b), all the acoustic eigenwaves manifest no significant anisotropy in the *ab* plane. The lowest velocity for the

Table 2. Elastic-stiffness and compliance coefficients calculated for $TlInSe_2$.

ij	11	33	12	13	44	66
C_{ij} (10^9 N/m^2)	42.11 ± 0.45	83.54 ± 0.69	12.59 ± 0.98	8.93 ± 1.61	11.88 ± 0.22	11.24 ± 0.21
S_{ij} (10^{-12} m^2/N)	26.41 ± 0.53	12.40 ± 0.19	−7.47 ± 0.77	−2.03 ± 0.39	84.19 ± 1.52	88.98 ± 1.69

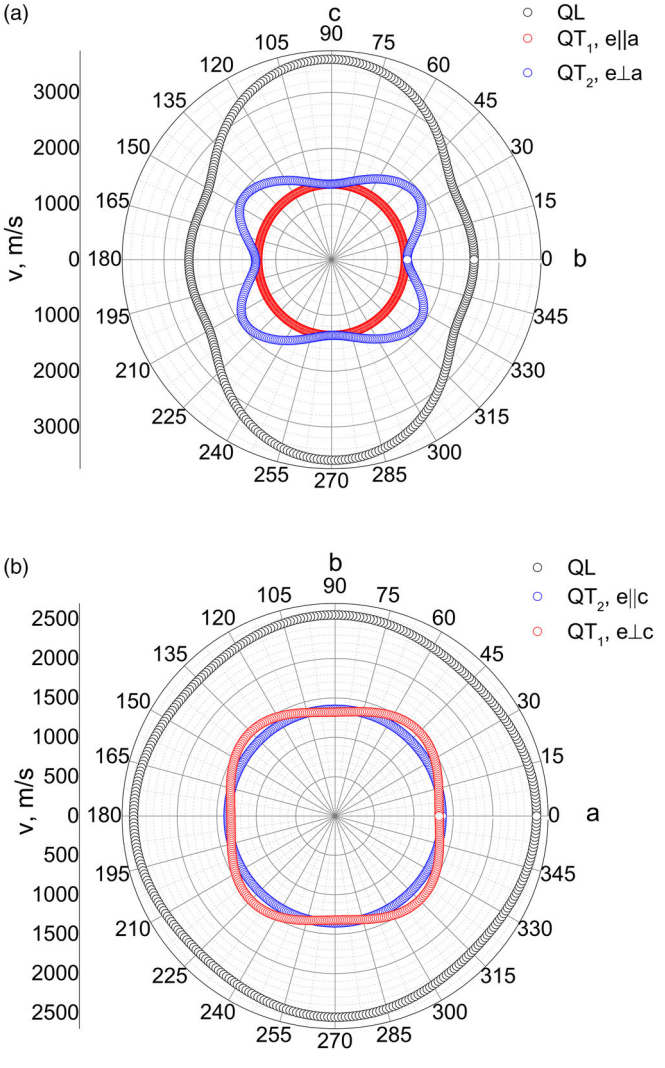

Figure 2. Cross sections of AW velocity surfaces by the crystallographic planes *bc* (a) and *ab* (b), as calculated for $TlInSe_2$: *e* denotes the displacement vector.

QL waves, 2444 m/s, is reached in the case when the AW propagates along bisector between the *a* and *b* axes (Figure 2(b)). The lowest velocity for the QT_1 and QT_2 waves is equal to 1356 m/s when the QT_1 wave propagates along arbitrary directions inside the *bc* plane (Figure 2(a)), or when the QT_2 wave propagates in any direction inside the *ab* plane (Figure 2(b)) or along the *c* axis (Figure 2(a)). The crystallographic axes *a*, *b* and *c* represent the acoustic axes for the transverse AWs. Under propagation along these directions, the velocities of transverse eigenwaves are the same (see Figure 2). Thus, $TlInSe_2$ has three acoustic axes under normal conditions.

As seen from Figure 3(a), the obliquity angle for the QT_2 and QL waves acquires high enough values in the *bc* plane. This angle is 40.7° when the wave vector of the AW QT_2 makes the angle 18° with respect to the *b* axis. When the orientation angle of the QL wave vector is 45° with respect to the *b* axis in the *bc* plane, the obliquity angle is 28.6°. The obliquity angles for the QT_1 waves do not exceed 1.5° in this plane. At the same time, the AW QT_1 is characterized by large obliquity in the *ab* plane (see Figure 3(b)). Consequently, we have $\pm 15.2°$ at the wave vector orientations given by the angles 23° and 69° with respect to the *a* axis. Finally, the obliquity angles for the QL waves in the

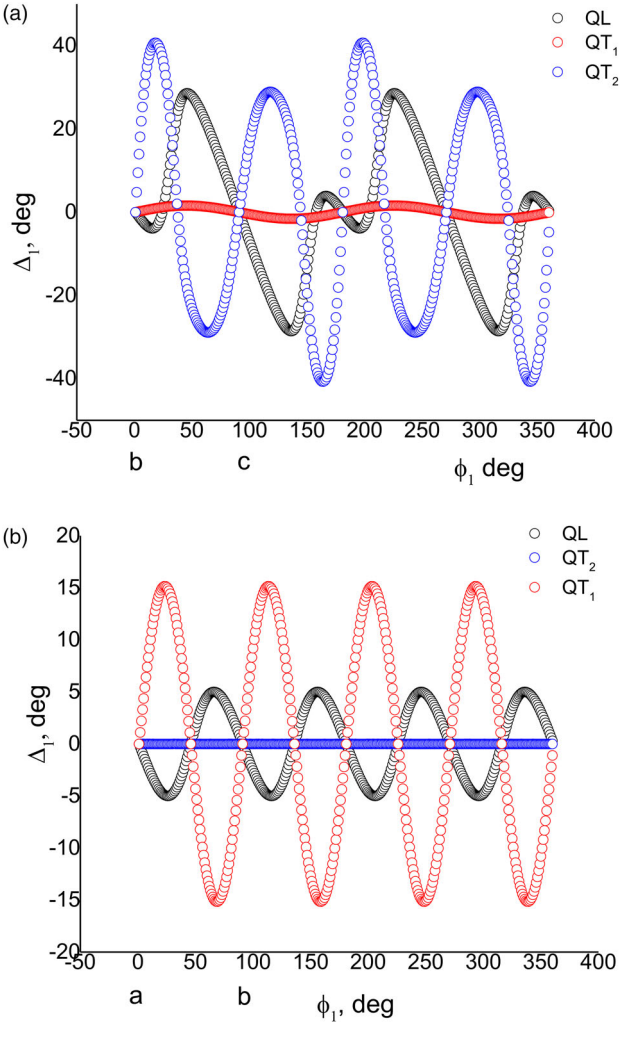

Figure 3. Dependences of obliquity angle of AW energy propagation on the direction of AW vector in the *bc* (a) and *ab* (b) planes, as calculated for $TlInSe_2$.

ab plane are quite small (~5.0°) and the effect in this plane is completely absent for the AW QT_2 (see Figure 3(b)).

As seen from Figure 4(a), the angle of deviation from the purely transverse or longitudinal polarization states in the *bc* plane reaches the value 22.8° when the AW vector is oriented under the angle 48° with respect to the *b* axis in the *bc* plane (the cases of the AWs QT_2 and QL). It is equal to ±7.7° when the AW vector is oriented under the angles 19° or 71° with respect to the *a* axis in the *ab* plane (the cases of the AWs QT_2 and QL – see Figure 4(b)).

The angle of deviation from the purely transverse or longitudinal polarization states and the obliquity angle are a measure of crystal anisotropy. For example, in a so-called isotropic approximation ($C_{11} = C_{33}$, $C_{12} = C_{13}$ and $C_{44} = C_{66} = (C_{11} - C_{12})/2$) it follows from Equations (4) and (5) that the angle of deviation from the purely transverse or longitudinal polarization states vanishes. The same concerns the obliquity angle defined by a general relation given by Equation (3).

The temperature dependences of the AW velocities v_{11}, v_{22} and v_{33} and the appropriate elastic-stiffness coefficients C_{11}, C_{22} and C_{33} are shown in Figure 5(a,b), respectively. We find $C_{11} = C_{22}$

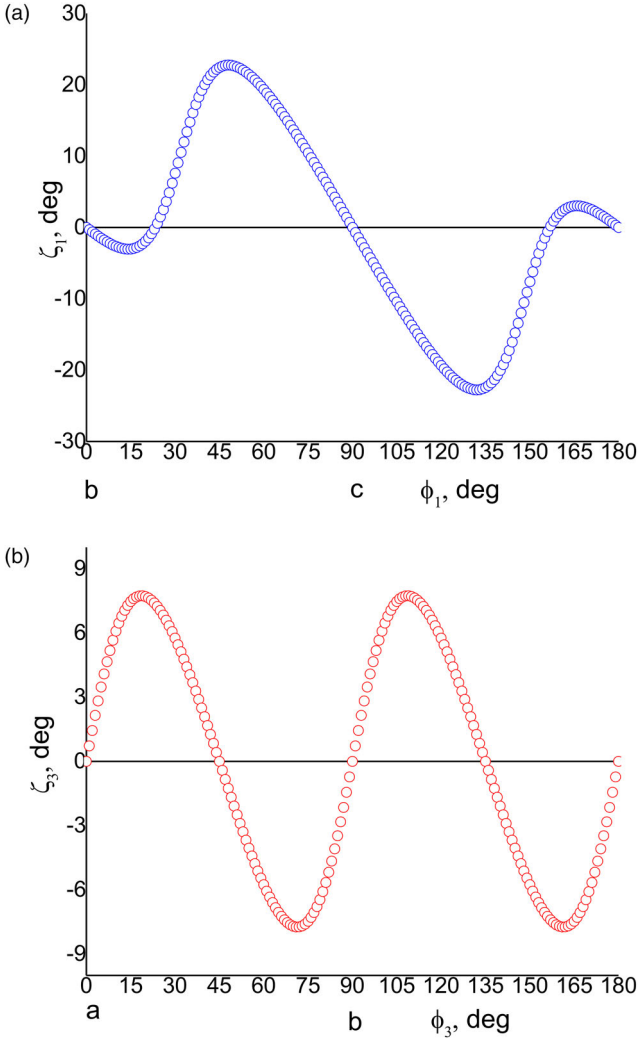

Figure 4. Dependences of the angle of deviation from purely transverse and longitudinal polarization states on the direction of AW vector in $TlInSe_2$, as calculated for the AWs QL and QT_2 in the *bc* plane (a) and for the AWs QL and QT_1 in the *ab* plane (b).

for crystals belonging to the tetragonal point symmetry group 4/mmm but not so for crystals of lower-symmetry systems, e.g. the orthorhombic. At temperatures below ca. 270 K, the temperature curves for the AW velocities and the elastic-stiffness coefficients are split, and a small break of these curves is observed at $T_1 \approx 245$ K (see Figure 5(a,b)). The measurements of the AW velocities in the temperature region below 166–185 K become difficult due to scattering of the AWs and disappearing of the reflected signal. This can be caused by diffusion of the phase transition in the vicinity of $T_2 \approx 145$ K, with the appearance of phase coexistence and nucleation of a domain structure. The reflected signal has not been clearly detected down to the lowest temperature of our measurements near 120 K.

Unfortunately, the data for the elasto-optic coefficients of $TlInSe_2$ are not available in the literature. Nevertheless, one can take the AOFM data from Ref. [22] ($M_2 = 156\times10^{-15}$ s^3/kg) and determine the component $p_{11} = p_{22}$ of the elasto-optic tensor from the formula $|p_{22}| = \sqrt{M_2 v_{22}^3 \rho / n_o^6}$. This AOFM value corresponds to the isotropic AO interaction with the longitudinal AW that propagates along the b axis (type 1 of AO interactions – see Figure 6). We find $|p_{22}| = 0.15$ for the optical wavelength 1.15 μm. As mentioned above, the slowest AW QL propagates along the bisector of the a and b axes. One of the possible isotropic interactions with this AW, which corresponds to the type 2 of AO interactions, is shown in Figure 6. Neglecting a small Bragg angle, we write the effective elasto-optic coefficient for this interaction type as $p_{ef} = (p_{11} + p_{12} + 2p_{66})/2$. Using the isotropic approximation and assuming that $p_{66} \approx (p_{11} - p_{12})/2$ we obtain $p_{ef} \approx p_{11}$. In this case, we derive

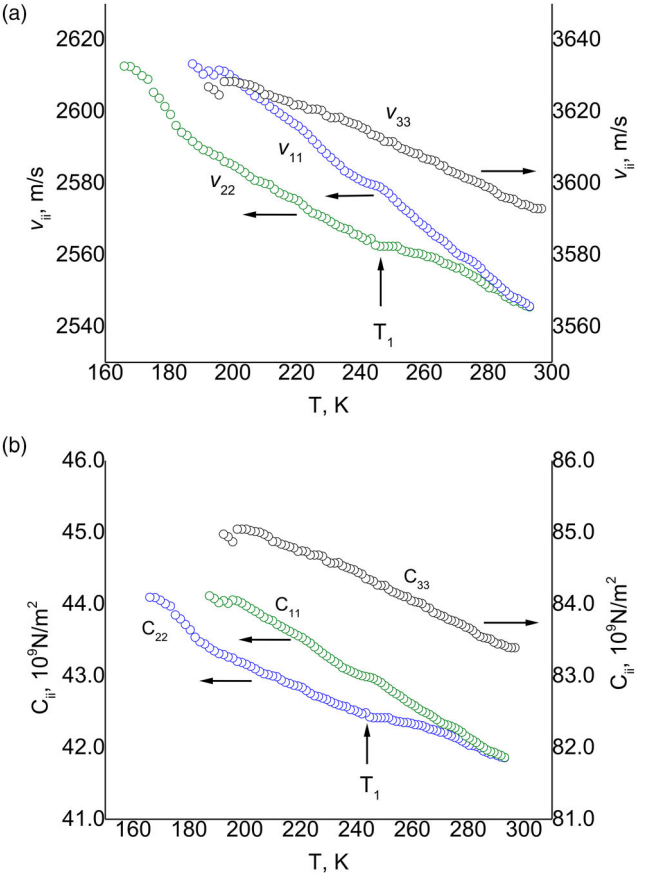

Figure 5. Temperature dependences of AW velocities v_{11}, v_{22} and v_{33} (a) and elastic-stiffness coefficients C_{11}, C_{22} and C_{33} (b) for $TlInSe_2$ crystals.

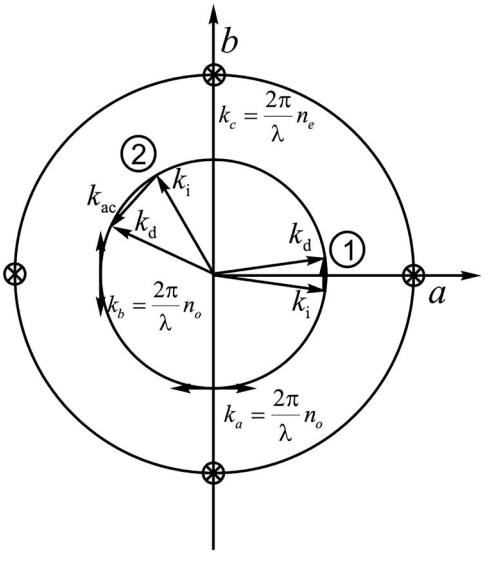

Figure 6. Schematic wave vector diagram for isotropic AO interactions with the AWs QL propagating along the *b* axis (1) and along bisector of the *a* and *b* axes in the *ab* plane. k_i and k_d denote the wave vectors of incident and diffracted optical waves, whereas K_{ac} is the AW vector. Double-sided arrows and crossed circles indicate polarizations of the optical waves.

a somewhat higher AOFM ($M_2 \approx 170 \times 10^{-15}$ s^3/kg), which is due to the increased slowness of the QL wave. However, one needs to know all of elasto-optic tensor components in order to perform a more reliable analysis of the AOFM anisotropy.

3.2. Thermal expansion anisotropy

The behaviour of the relative linear elongation (Figure 7(a)) and the volume thermal expansion (Figure 7(b)) are notably changed below $T_1 \approx 245$ K under cooling. This temperature is far removed from 185 K, which could be associated with the PT in the light of the earlier literature data. Nonetheless, it does follow from the temperature dependence of the lattice parameter *a* [17] that, with decreasing temperature, the lattice parameter in the vicinity of T_1 starts to deviate from a linear trend, in spite of the fact that the heat capacity measured in the same work reveals the anomaly at 185 K. The temperature curves of the relative elongations along the *a* and *b* axes are split at T_1 (see Figure 7(a)), thus indicating that the crystal symmetry becomes lower and corresponds to one of the orthorhombic symmetry groups.

However, a comparison of Figure 7(a,b) shows that a temperature decrease below T_1 leads to expansion along all of the three principal axes, which manifests itself in differences between the dashed lines and the experimental points corresponding to spontaneous strains. This fact is unusual for ferroic crystals where the PTs are accompanied by lattice strains since the trace of the spontaneous strain tensor should be equal to zero [33] avoiding changes of the unit-cell volume. In fact, we have observed a change of the volume expansion at T_1 (see Figure 7(b)), which is given by a difference of the dashed line and the data represented by experimental points. Notice also that the volume thermal expansion is almost independent of temperature between the points T_1 and $T_2 \approx 145$ K (i.e. the volume thermal expansion coefficient is equal to zero – see Figure 8(b)), although the sample starts to expand sharply below T_2.

The linear thermal expansion coefficients at $T = 290$ K are equal to $\alpha_{aa} = (3.3 \pm 0.7) \times 10^{-5}\text{K}^{-1}$, $\alpha_{bb} = (2.3 \pm 0.7) \times 10^{-5}\text{K}^{-1}$ and $\alpha_{cc} = (0.4 \pm 0.7) \times 10^{-5}\text{K}^{-1}$ (see Figure 8(a)). Taking the experimental errors into account, we conclude that the components α_{aa} and α_{bb} are equal to each

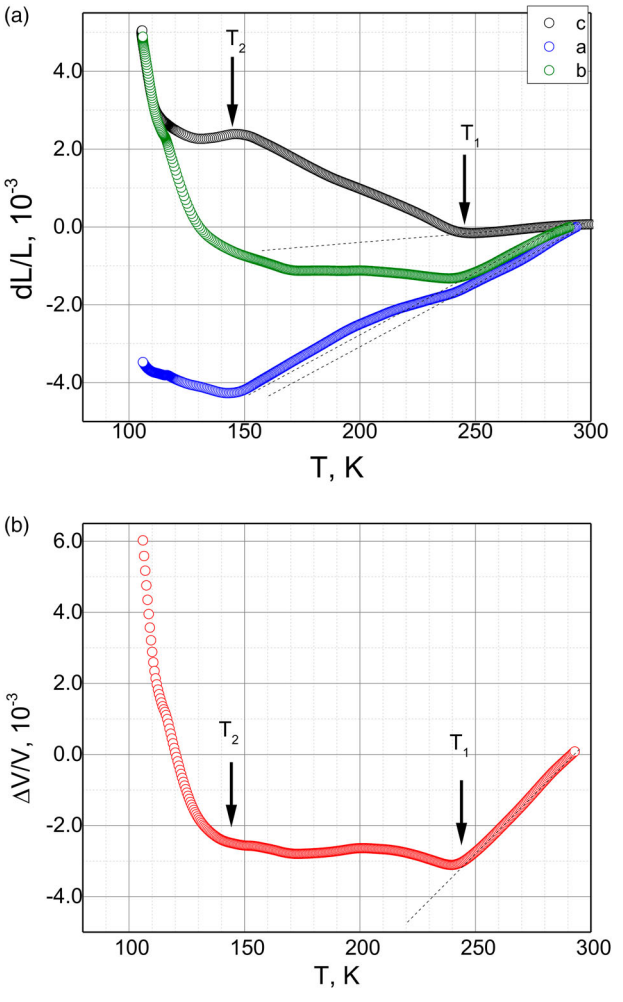

Figure 7. Temperature dependences of relative linear elongation (a) and volume thermal expansion (b) for $TlInSe_2$. Dashed lines correspond to linear extrapolation from the region $T > 245$ K.

other both at the normal conditions and above the temperature point T_1. However, the linear thermal expansion curves α_{aa} and α_{bb} are split as the temperature decreases below T_1. Below T_2, the linear thermal expansion coefficients and the volume thermal expansion coefficient (see Figure 8(b)) become negative and increase in modulus almost two orders of magnitude. Such an abrupt variation of these parameters testifies some structural changes that occur below the temperature point T_2, as well as a lowered symmetry of $TlInSe_2$ below T_1.

4. Conclusions

Based on the comprehensive studies of the AW velocities, we have determined all components of the elastic-stiffness and compliance tensors for $TlInSe_2$ crystals. It has been found that the elastic compliances $S_{44} = S_{55}$ and S_{66} are much larger than other tensor components, thus testifying an extremely high compliance of $TlInSe_2$ with respect to shear stresses. Using the cross sections of the AW velocity surfaces, we have found that $TlInSe_2$ contains three acoustic axes parallel to the principal crystallographic directions. The lowest velocities of the acoustic eigenwaves have been determined. The lowest velocity for the QL waves, 2444 m/s, is reached when the AW propagates along the bisector of the

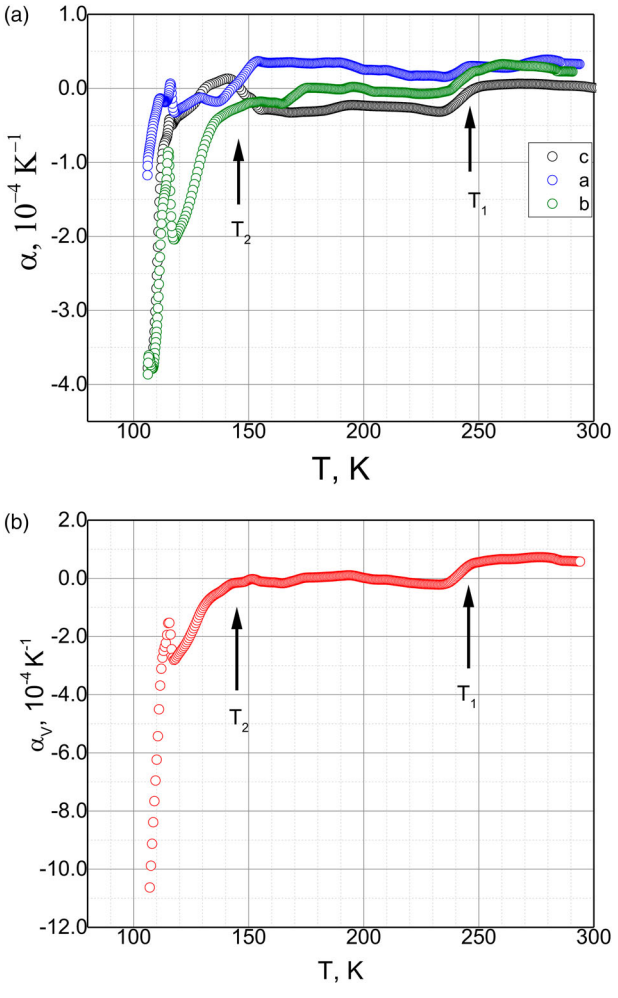

Figure 8. Temperature dependences of linear (a) and volume (b) thermal expansion coefficients for $TlInSe_2$.

a and *b* axes. The lowest velocity for the QT_1 and QT_2 waves is equal to 1356 m/s. It corresponds to the QT_1 wave propagating along arbitrary direction inside the *bc* plane, as well as the QT_2 wave propagating in any direction in the *ab* plane, or along the *c* axis. The AOFM has been estimated for the case of AO interactions with the slowest QL wave. It has been shown that the angle between the direction of the acoustic energy flow and the AW vector in $TlInSe_2$ is high enough. The same is true of the angle of deviation of AW polarization from the purely longitudinal or transverse states.

We have studied the temperature behaviour of the relative elongation along the three principal crystallographic directions. The corresponding dependences of the thermal expansion coefficients have been obtained. The linear thermal expansion coefficients at $T = 290$ K are equal to $\alpha_{aa} = (3.3 \pm 0.7) \times 10^{-5}\mathrm{K}^{-1}$, $\alpha_{bb} = (2.3 \pm 0.7) \times 10^{-5}\mathrm{K}^{-1}$ and $\alpha_{cc} = (0.4 \pm 0.7) \times 10^{-5}\mathrm{K}^{-1}$. Anomalous behaviour of these parameters has been detected at $T_1 \approx 245$ K and $T_2 \approx 145$ K. Unfortunately, we cannot make clear conclusions on the origin of structural changes that appear at the T_1 and T_2 points in $TlInSe_2$ basing on the results presented in this study. Nonetheless, following from the temperature dependences of the AW velocities and the thermal expansion data, we conclude that the symmetry of $TlInSe_2$ becomes lower than tetragonal one below the T_1 point. Along with the appearance of spontaneous strains along the principal crystallographic directions, this can point to a ferroelastic nature of the PT. Moreover, there can be phase coexistence in the

temperature region between the T_1 and T_2 points. Notice that a specific temperature point $T_2 \approx 145$ K is detected close to the temperature $T = 135$ K where the phase transition from the IC phase to the ordered phase has been detected [17–21]. The point $T_1 \approx 245$ K may correspond to the temperature 185 K supposed to be at a PT [17]. Increased scattering of the AWs has been found at 185 K. As follows from the smooth anomalies of AW velocities, the AW scattering, the relative elongation and the thermal expansion coefficients measured in the present work, we conclude that $TlInSe_2$ undergoes several phase transitions and passes through a wide temperature range of phase coexisting.

Disclosure statement

No potential conflict of interest was reported by the authors.

Funding

The authors acknowledge financial support of the present study from the Ministry of Education and Science of Ukraine (the Project #0117U006454).

References

[1] Panich AM. Electronic properties and phase transitions in low-dimensional semiconductors. J Phys: Condens Matter. 2008;20:293202.
[2] Kashida S, Kobayashi Y. X-ray study of the incommensurate phase of $TlInS_2$. J Phys: Condens Matter. 1999;11:1027–1035.
[3] Delgado GE, Mora AJ, Perez FV, et al. Crystal structure of the ternary semiconductor compound thallium gallium sulfide, $TlGaS_2$. Physica B. 2007;391:385–388.
[4] Gasanly NM, Marvin BN, Sterin KE, et al. Raman study of layer TlGaS2, β-TlInS2, and TlGaSe2 crystals. Phys Status Solidi (b). 1978;86:K49–K53.
[5] Muller D, Eulenberger G, Hahn H. Über ternäre Thalliumchalkogenide mit Thalliumselenidstruktur. Z Anorg Allg Chem. 1973;398:207–220.
[6] Salnik A, Gololobov YP, Borovoy NA. The incommensurate phase transformation in $TlInS_2$ ferroelectric. Ferroelectrics. 2015;484:62–68.
[7] Volkov AA, Goncharov YG, Kozlov GV, et al. Structural phase transitions in $TlInS_2$ crystal. Sov Phys: Solid State. 1983;25:2061–2062.
[8] Gololobov YP, Borovoy NA, Isayenko GL, et al. Ferroelectric phases in the polytypes of $TlInS_2$ ternary compound. Phys Status Solidi (c). 2009;6:989–992.
[9] Alekperov OZ, Ibragimov GB, Nadjafov AI, et al. Polytypes in ferroelectric $TlInS_2$ and its dielectric and optic properties. Phys Status Solidi (c). 2009;6:977–980.
[10] Say A, Martynyuk-Lototska I, Adamenko D, et al. Thermal expansion anisotropy of β-$TlInS_2$ crystals in the course of phase transitions. Phase Trans. 2017;91(1):1–8.
[11] Aliev VA, Aldzhanov MA, Aliev SN. Incommensurate phase transition in $TlGaTe_2$. JETP Lett. 1987;45:534–536.
[12] Banys J, Wondre FR, Guseinov G. Powder diffraction study of TlGaTe2, TlInTe2 and TlInSe2. Mater Lett. 1990;9:269–274.
[13] Mamedov NT, Panich AM. Phase transition in $TlGaTe_2$. Phys Status Solidi (a). 1990;117:K15–K17.
[14] Mamedov KK, Abdullaev M, Kerimova EM. Heat capacities of $TlInS_2$ and $TlInSe_2$ crystals at low temperatures. Phys Status Solidi (a). 1986;94:115–119.
[15] Sheleg AU, Hurtavy VG, Shautsova VV, et al. Dielectric properties and phase transitions in crystals of $TlInS_xSe_{2-x}$ solid solutions. Sov Phys: Solid State. 2012;54:622–625.
[16] Sheleg AU, Zub EM, Yachkovskii AY, et al. X-ray diffraction study of $(TlInSe_2)_{1-x}(TlGaTe_2)_x$ crystal system. Crystallogr Rep. 2012;57:283–285.
[17] Alekperov OZO, Aljanov MAO, Kerimova EMAG. Low-temperature phase transition in $TlInSe_2$ crystals. Tr J Phys. 1998;22:1053–1058.
[18] Hosokawa S, Kamimura K, Ikemoto H, et al. Structural studies on TlInSe2 thermoelectric material by X-ray fluorescence holography, XAFS, and X-ray diffraction. Phys Status Solidi (b). 2015;252:1225–1229.
[19] Hosokawa S, Stellhorn JR, Ikemoto H, et al. Lattice distortions in $TlInSe_2$ thermoelectric material studied by X-ray absorption fine structure. Phys Status Solidi (a). 2017; 215:1700416.

[20] Ishikawa M, Nakayama T, Wakita K, et al. First-principles study of giant thermoelectric power in incommensurate $TlInSe_2$. J Appl Phys. 2018;123:161575.
[21] Mimura K, Nogami T, Abe K, et al. Temperature-dependent angle-resolved photoemission spectra of $TlInSe_2$: manifestations of incommensurate and commensurate phases. Jpn J Appl Phys. 2008;47:8188.
[22] Gottlieb M, Isaacs TJ, Feichtner JD, et al. Acoustooptic properties of some chalcogenide crystals. J Appl Phys. 1974;45:5145–5151.
[23] Martynyuk-Lototska I, Trach I, Kokhan O, et al. Efficient acousto-optic crystal, $TlInS_2$: acoustic and elastic anisotropy. Appl Opt. 2017; 56: 3179–3184.
[24] Mys O, Kryvyy T, Mytsyk B, et al. Acoustooptic figure of merit of Tl_3AsS_4 crystals. The case of acoustic waves propagation along crystallographic axes. Ukr J Phys Opt. 2018;19:99–105.
[25] Mys O, Krupych O, Vlokh R. Anisotropy of acoustooptic figure of merit in KH_2PO_4 crystals. Ukr J Phys Opt. 2017;18:83–94.
[26] Mys O, Krupych O, Vlokh R. Anisotropy of an acousto-optic figure of merit for $NaBi(MoO_4)_2$ crystals. Appl Opt. 2016;55:7941–7955.
[27] Allakhveriev KR, Mamedov TG, Salaev EY, et al. The fundamental absorption edge of $TlInSe_2$. Phys Status Solidi (b). 1982;113:K43–K47.
[28] Kurbanov MM, Bairamov DD, Sardarova NS. Thermal expansion of TllnXz (X = S, Se, Te). Inorg Mater. 2000;36:132–133.
[29] Mamedov N, Wakita K, Shim Y, et al. Temperature-dependent and pump-probe ellipsometric studies of $TlInSe_2$. Thin Solid Films 2008;517:1434–1438.
[30] Papadakis E. Ultrasonic phase velocity by the pulse-echo-overlap method incorporating diffraction phase corrections. J Acoust Soc Am. 1967;42:1045–1051.
[31] Ohmachi Y, Uchida N, Niizeki N. Acoustic wave propagation in TeO_2 single crystals. J Acoust Soc Am. 1972;51:164–168.
[32] Shaskolskaya MP. Acoustic crystals. Moscow: Nauka; 1982.
[33] Sapriel J. Domain-wall orientations in ferroelastics. Phys Rev B 1975;12:5128–5140.